Figure S1: Related to Figure 1.

(A) AF2 model and PAE plot of the CDR2 N-terminal coiled-coil in complex with the DLIC1 C-terminal helix and an N-terminal DHC fragment, which in turn is bound to the WD40 domain of DIC2.

(B) Sequence alignment of the CC1 box and the dynein heavy chain binding site 1 (HBS1) in CDR2 and CDR2L proteins from different species (note invertebrates possess a single CDR2/CDR2L homolog). The HBS1 sequence is divergent from that of other adaptors but the interaction is predicted at the correct distance from the CC1 box. 6 residues, marked with asterisks, were mutated to alanine (HBS1_6A mutant) based on sequence conservation among CDR2 proteins and their position in the predicted structure. Accession numbers: CDR2_HUMAN (UniProt Q01850), CDR2L_HUMAN (UniProt Q86X02), CDR2_MOUSE (UniProt P97817), CDR2L_MOUSE (UniProt A2A6T1), CDR2_XENTR (UniProt F6R4S1), CDR2L_XENTR (UniProt A0A803JSM3), CDR2_DANRE (UniProt E7FC97), CDR2L_DANRE (UniProt Q6NZT2),

CDR2_BRABE (UniProt A0A6P4ZS94), CDR2_SACKO (NCBI Reference Sequence XP_002736317.2), CDR2_STRPU (UniProt A0A7M7NRE1), CDR2_LINAN (NCBI Reference Sequence XP_013392376.1), CEN_DROME (UniProt Q9VIK6), CDR2_HYDVU (UniProt A0A8B6XII3). Species key (Phylum): HUMAN, *Homo sapiens* (Chordata); MOUSE, *Mus musculus* (Chordata); XENTR, *Xenopus tropicalis* (Chordata); DANRE, *Danio rerio* (Chordata); BRABE, *Branchiostoma belcheri* (Chordata); SACKO, *Saccoglossus kowalevskii* (Hemichordata); STRPU, *Strongylocentrotus purpuratus* (Echinodermata); LINAN, *Lingula anatina* (Brachiopoda); DROME, *Drosophila melanogaster* (Arthropoda); HYDVU, *Hydra vulgaris* (Cnidaria).

(C) Elution profiles and BlueSafe-stained SDS-PAGE gels of purified recombinant human CDR2 and DLIC1 fragments after SEC. DLIC1-C corresponds to residues 388-523. The elution profile and gel for CDR2 are shown on both left and right to facilitate comparison between wild-type DLIC1-C and the F447A/F448A mutant. Molecular weight is indicated in kilodaltons (kDa).

Figure S2: Related to Figure 2.

(A) Immunoblots of HeLa cells harboring single and double KOs of CDR2 and CDR2L (two independently derived cell lines were analyzed for each condition). GAPDH serves as the loading control. Molecular weight is indicated in kilodaltons (kDa).

(B) Immunoblots of CDR2/L double KO cells stably expressing GFP::3xFLAG::CDR2 or CDR2L, used for the experiments in *Fig. 2A*. GAPDH serves as the loading control. Molecular weight is indicated in kilodaltons (kDa).

(C) Immunofluorescence of CDR2/L double KO cells stably expressing GFP::3xFLAG::CDR2L, showing co-localization with KTN1 and diffuse cytoplasmic signal. Note that while average expression levels of transgene-encoded CDR2L are significantly higher than those of endogenous CDR2L, as shown in *(B)*, expression in individual cells is variable. Cells shown here have relatively low expression levels. Scale bar, 10 μm.

(D) Sequence alignment of the C-terminal helix in CDR2 and CDR2L proteins from different species. Accession numbers and species key as in *Fig. S1B*.

(E)–(G) Immunofluorescence images and immunoblots showing knockdown of KTN1 by RNAi and the resulting delocalization/destabilization of CDR2 in HeLa cells. By contrast, KTN1 levels remain unaffected in CDR2/L double KO cells (two independently derived KO cell lines were analyzed). Scale bars, 20 μm *(E)* and 10 μm *(F)*. Molecular weight is indicated in kilodaltons (kDa).

(H) Sequence alignment of the CDR2/eEF1Bβ binding site in KTN1 and its paralog RRBP1 (p180) from different species (invertebrates possess a single KTN1/RRBP1 homolog). Accession numbers: KTN1_HUMAN (UniProt Q86UP2), RRBP1_HUMAN (Q9P2E9), KTN1_MOUSE

(UniProt Q61595), RRBP1_MOUSE (UniProt Q99PL5), KTN1_XENTR (UniProt B3DL66), RRBP1_XENTR (UniProt F7A6K6), KTN1_DANRE (UniProt E7F049), RRBP1_DANRE (UniProt B8A4D7), RRBP1_BRABE (UniProt A0A6P5A3T7), RRBP1_SACKO (NCBI Reference Sequence XP_002741373.1), RRBP1_STRPU (A0A7M7LVI4), KTN1_LINAN (NCBI Reference Sequence XP_013397491.1). Species key as in *Fig. S1B*. No CDR2 binding site could be identified for the KTN1/RRBP1 homologs of DROME and HYDVU (UniProt Q960Y8 and T2M451, respectively), despite the presence of a well conserved CDR2 helix, as shown in *(D)*.

Figure S3: Related to Figures 3, 4 and 5.

(A) *(left)* Immunofluorescence images showing exacerbated patchy distribution of KTN1 in HeLa CDR2/L double KO cells. Scale bar, 20 µm. *(right)* Fraction of cells with prominent KTN1 patches, plotted as mean ± SD (4 independent experiments, >1000 cells scored in total per condition). Statistical significance was determined using a two-tailed t test. ****$P < 0.0001$. These cells were treated with siRNA against Luciferase, which further enhances KTN1 patch formation in CDR2/L double KO cells relative to untreated cells (compare with quantification in *Fig. 3A*).

(B) Correlative light–electron microscopy images of CDR2/L double KO cells showing that the KTN1 patches observed by immunofluorescence correspond to stacked ER sheets. Scale bars, 5 µm *(top)* and 1 µm *(bottom)*.

(C) Fraction of cells (mean ± SD, 4 and 3 independent experiments for ΔCC1 box and ΔHelix, respectively; >580 cell scored in total per condition) with prominent KTN1 patches *(left)* or centrosome-proximal KTN1 clustering *(right)* in the conditions shown in *Fig. 3E*, using a second independently derived CDR2/L double KO cell line. ΔCC1 box and ΔHelix experiments each have their own WT and GFP-negative controls. Statistical significance was determined using ordinary one-way ANOVA followed by Tukey's multiple comparisons test. ****$P < 0.0001$; **$P < 0.01$; *ns* = not significant, $P > 0.05$.

(D) *(left)* TEM images of ER sheets in CDR2/L double KO cells with and without knockdown of KTN1. Scale bar, 1 µm. *(right)* Number of ER sheets in the largest stack per cell, determined as described in *Fig. 3B*. The CDR2/L double KO data is the same as in *Fig. 3B*.

(E) Immunofluorescence image showing penetrant and tight clustering of KTN1 in the presence of JIP3(1–185)::CDR2(186–454). Scale bar, 10 µm.

(F) AF2 model and predicted alignment error (PAE) plot of full-length eEF1Bβ in complex with the KTN1 C-terminus. One copy of eEF1Bβ was used for the prediction, but note that eEF1Bβ can form a trimer through its leucine zipper (LZ) domain (Bondarchuk *et al.*, 2022).

(G) Immunofluorescence images (maximum intensity projection of z-stack) showing that eEF1Bβ knockdown in CDR2/L double KO cells does not alter KTN1 distribution (see corresponding quantification in *Fig. 5C*). Scale bar, 10 μm.

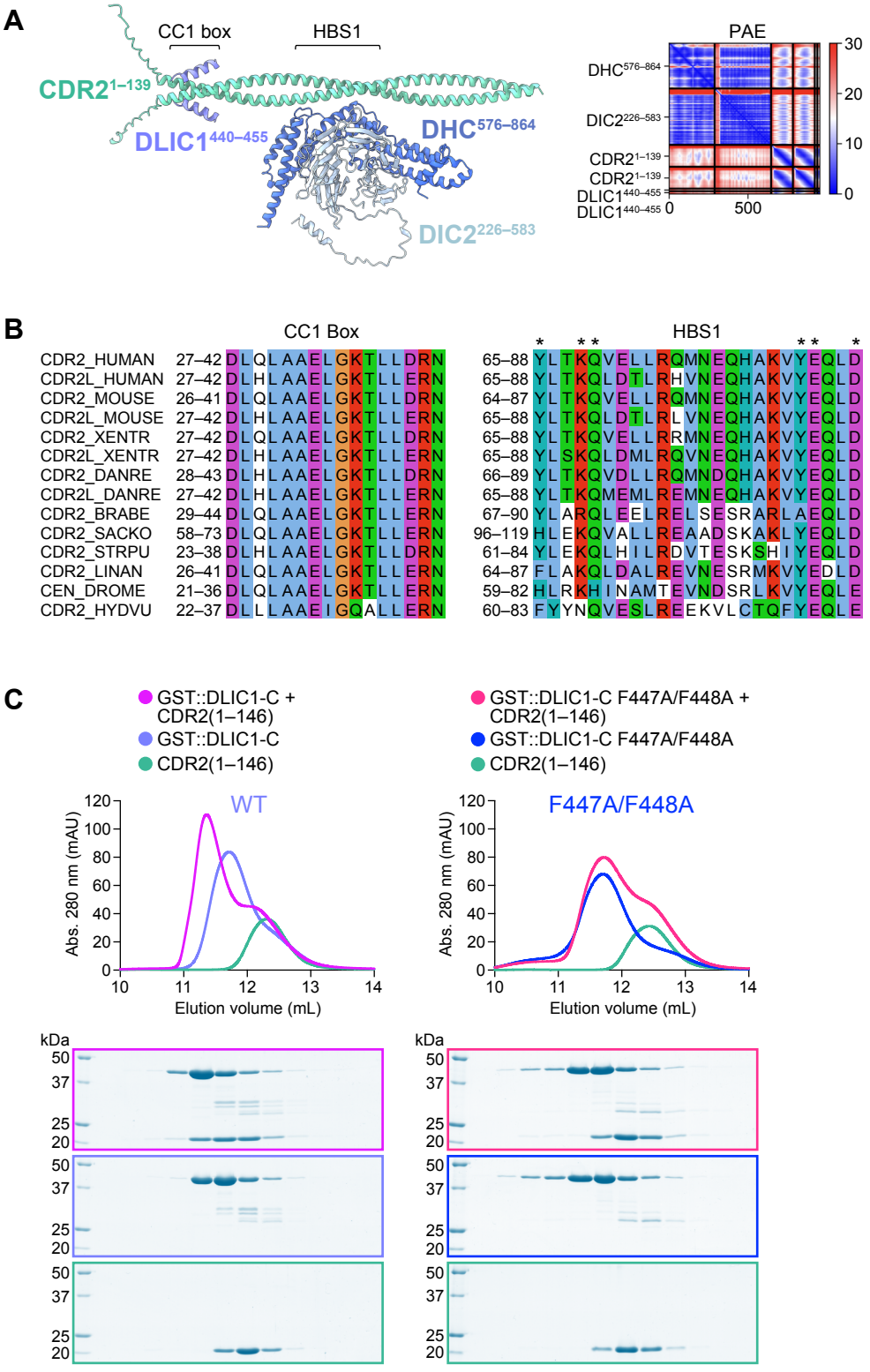
A
CC1 box
HBS1
CDR2 1–139
DLIC1 440–455
DHC 576–864
DIC2 226–583
PAE
DHC 576–864
DIC2 226–583
CDR2 1–139
CDR2 1–139
DLIC1 440–455
DLIC1 440–455
0
500
30
20
10
0
B
CC1 Box
HBS1
CDR2_HUMAN 27–42 DLQLAAELGKTLLDRN 65–88 YLTKQVELLRQMNEQHAKVYEQLD
CDR2L_HUMAN 27–42 DLHLAAELGKTLLERN 65–88 YLTKQLDTLRHVNEQHAKVYEQLD
CDR2_MOUSE 26–41 DLQLAAELGKTLLDRN 64–87 YLTKQVELLRQMNEQHAKVYEQLD
CDR2L_MOUSE 27–42 DLHLAAELGKTLLERN 65–88 YLTKQLDTLRLVNEQHAKVYEQLD
CDR2_XENTR 27–42 DLQLAAELGKTLLDRN 65–88 YLTKQVELLRRMNEQHAKVYEQLD
CDR2L_XENTR 27–42 DLHLAAELGKTLLERN 65–88 YLSKQLDMLRQVNEQHAKVYEQLD
CDR2_DANRE 28–43 DLHLAAELGKTLLDRN 66–89 YLTKQVDLLRQMNDQHAKVYEQLD
CDR2L_DANRE 27–42 DLHLAAELGKTLLERN 65–88 YLTKQMEMLREMNEQHAKVYEQLD
CDR2_BRABE 29–44 DLQLAAELGKTLLERN 67–90 YLARQLEELRELSESRARLAEQLD
CDR2_SACKO 58–73 DLQLAAELGKTLLERN 96–119 HLEKQVALLREAADSKAKLYEQLD
CDR2_STRPU 23–38 DLHLAAELGKTLLDRN 61–84 YLEKQLHILRDVTESKSHIYEQLD
CDR2_LINAN 26–41 DLQLAAELGKTLLERN 64–87 FLAKQLDALREVNESRMKVYEDLD
CEN_DROME 21–36 DLQLAAELGKTLLERN 59–82 HLRKHINAMTEVNDSRLKVYEQLE
CDR2_HYDVU 22–37 DLLLAAEIGQALLERN 60–83 FYYNQVESLREEKVLCTQFYEQLE
C
GST::DLIC1-C + CDR2(1–146)
GST::DLIC1-C
CDR2(1–146)
GST::DLIC1-C F447A/F448A + CDR2(1–146)
GST::DLIC1-C F447A/F448A
CDR2(1–146)
WT
F447A/F448A
Abs. 280 nm (mAU)
Elution volume (mL)
kDa
50
37
25
20

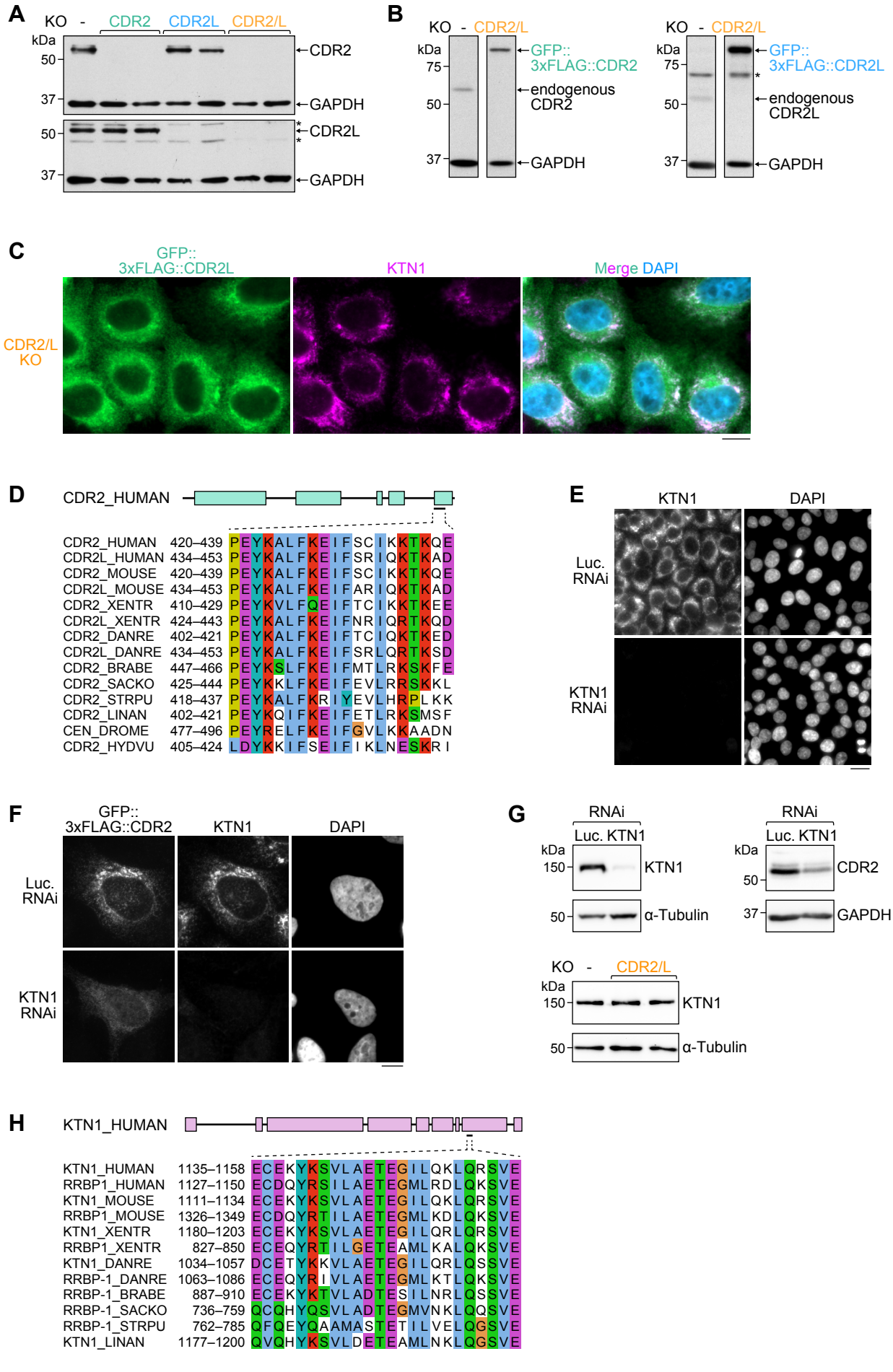
A
KO - CDR2 CDR2L CDR2/L
kDa
50
37
CDR2
GAPDH
50
37
CDR2L
GAPDH
B
KO - CDR2/L
kDa
75
50
37
GFP::
3xFLAG::CDR2
endogenous
CDR2
GAPDH
KO - CDR2/L
kDa
75
50
37
GFP::
3xFLAG::CDR2L
endogenous
CDR2L
GAPDH
C
GFP::
3xFLAG::CDR2L
KTN1
Merge DAPI
CDR2/L
KO
D
CDR2_HUMAN
CDR2_HUMAN 420–439 PEYKALFKEIFSCIKKTKQE
CDR2L_HUMAN 434–453 PEYKALFKEIFSRIQKTKAD
CDR2_MOUSE 420–439 PEYKALFKEIFSCIKKTKQE
CDR2L_MOUSE 434–453 PEYKALFKEIFARIQKTKAD
CDR2_XENTR 410–429 PEYKVLFQEIFTCIKKTKEE
CDR2L_XENTR 424–443 PEYKALFKEIFNRIQRTKQD
CDR2_DANRE 402–421 PEYKALFKEIFTCIQKTKED
CDR2L_DANRE 434–453 PEYKALFKEIFSRLQRTKSD
CDR2_BRABE 447–466 PEYKSLFKEIFMTLRKSKFE
CDR2_SACKO 425–444 PEYKKLFKEIFEVLRRSKKL
CDR2_STRPU 418–437 PEYKALFKRIYEVLHRPLKK
CDR2_LINAN 402–421 PEYKQIFKEIFETLRKSMSF
CEN_DROME 477–496 PEYRELFKEIFGVLKKAADN
CDR2_HYDVU 405–424 LDYKKIFSEIFIKLNESKRI
E
KTN1
DAPI
Luc.
RNAi
KTN1
RNAi
F
GFP::
3xFLAG::CDR2
KTN1
DAPI
Luc.
RNAi
KTN1
RNAi
G
RNAi
Luc. KTN1
kDa
150
50
KTN1
α-Tubulin
RNAi
Luc. KTN1
kDa
50
37
CDR2
GAPDH
KO - CDR2/L
kDa
150
50
KTN1
α-Tubulin
H
KTN1_HUMAN
KTN1_HUMAN 1135–1158 ECEKYKSVLAETEGILQKLQRSVE
RRBP1_HUMAN 1127–1150 ECDQYRSILAETEGMLRDLQKSVE
KTN1_MOUSE 1111–1134 ECEKYKSVLAETEGILQKLQRSVE
RRBP1_MOUSE 1326–1349 ECDQYRTILAETEGMLKDLQKSVE
KTN1_XENTR 1180–1203 ECEKYKSVLAETEGILQRLQRSVE
RRBP1_XENTR 827–850 ECEQYRTILGETEAMLKALQKSVE
KTN1_DANRE 1034–1057 DCETYKKVLAETEGILQRLQSSVE
RRBP-1_DANRE 1063–1086 ECEQYRIVLAETEGMLKTLQKSVE
RRBP-1_BRABE 887–910 ECEKYKTVLADTESILNRLQSSVE
RRBP-1_SACKO 736–759 QCQHYQSVLADTEGMVNKLQQSVE
RRBP-1_STRPU 762–785 QFQEYQAAMASTETILVELQGSVE
KTN1_LINAN 1177–1200 QVQHYKSVLDETEAMLNKLQGSVE

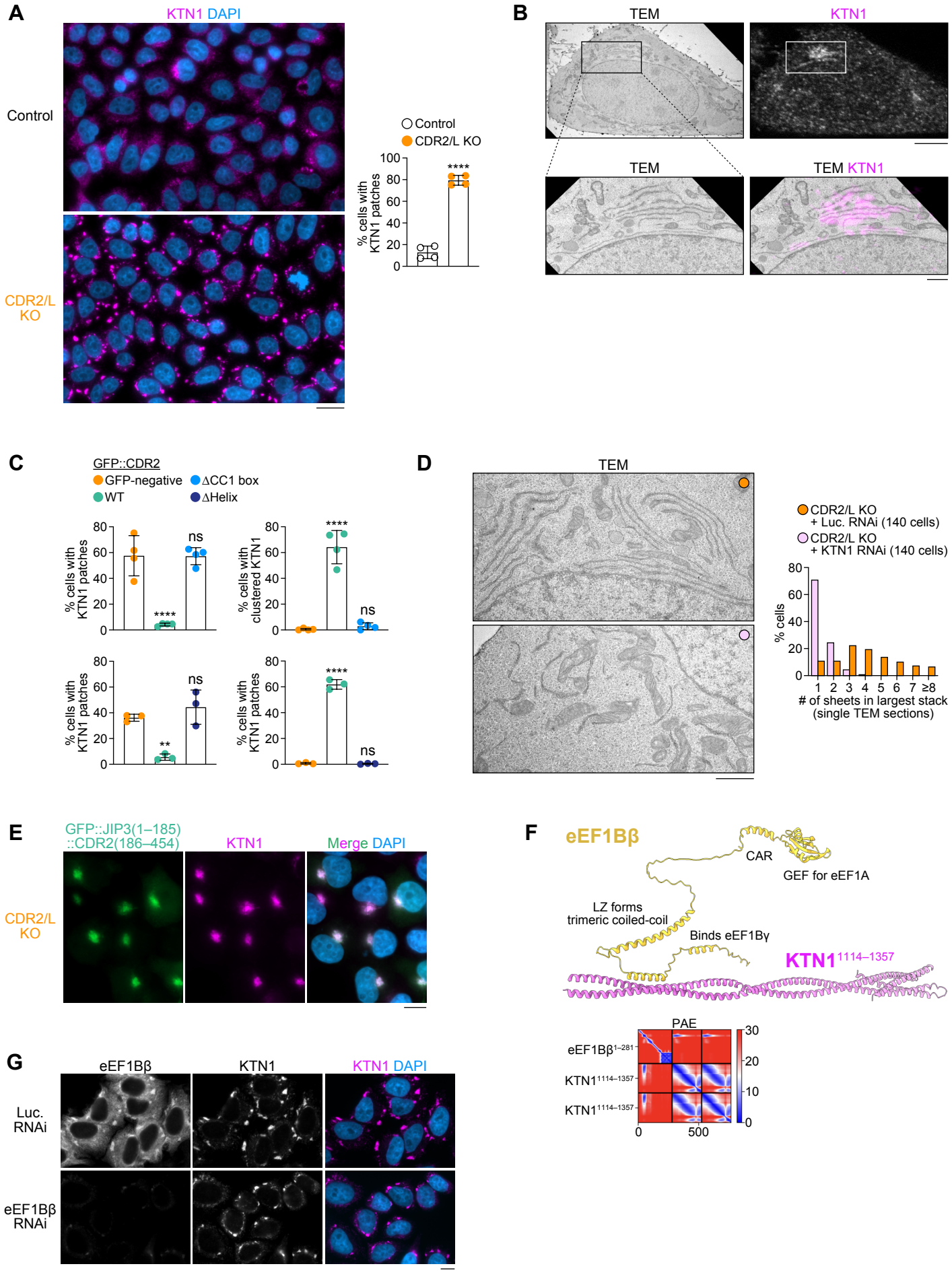
A
KTN1 DAPI
Control
CDR2/L KO
Control
CDR2/L KO
% cells with KTN1 patches
****
B
TEM
KTN1
TEM
TEM KTN1
C
GFP::CDR2
GFP-negative
ΔCC1 box
WT
ΔHelix
% cells with KTN1 patches
% cells with clustered KTN1
ns
****
**
D
TEM
CDR2/L KO + Luc. RNAi (140 cells)
CDR2/L KO + KTN1 RNAi (140 cells)
% cells
# of sheets in largest stack (single TEM sections)
E
GFP::JIP3(1–185) ::CDR2(186–454)
KTN1
Merge DAPI
CDR2/L KO
F
eEF1Bβ
CAR
GEF for eEF1A
LZ forms trimeric coiled-coil
Binds eEF1Bγ
KTN1 1114–1357
PAE
eEF1Bβ 1–281
KTN1 1114–1357
KTN1 1114–1357
G
eEF1Bβ
KTN1
KTN1 DAPI
Luc. RNAi
eEF1Bβ RNAi